Title

Spatio-temporal evolution of the L → H and H → L transitions

Journal

Nuclear Fusion, 53(7)

ISSN

0029-5515

Authors

Miki, K
Diamond, PH
Fedorczak, N
et al.

Publication Date

2013-07-01

DOI

10.1088/0029-5515/53/7/073044

Spatio-Temporal Evolution of the L→H and H→L Transitions

K. Miki[1], P.H. Diamond[1,2], N. Fedorczak[2], Ö.D. Gürcan[3], M. Malkov[2], C. Lee[2], Y. Kosuga[1,2,4], G. Tynan[2], G.S. Xu[5], T. Estrada[6], D. McDonald[7], L. Schmitz[8] and K.J. Zhao[1]

[1]WCI Center for Fusion Theory, NFRI, Daejeon 305-333, Korea.
[2]CMTFO, University of California, San Diego, La Jolla, CA 92093, USA.
[3]LPP, Ecole Polytechnique, CNRS, France.
[4]Institute for Advanced Study and Research Institute for Applied Mechanics, Kyushu University, Fukuoka, Japan
[5]Institute of Plasma Physics, Chinese Academy of Science, Hefei, China.
[6]Laboratorio National de Fusión, Associatión Euratom-CIEMAT, Madrid, Spain.
[7]EFDA, EU.
[8]University of California, Los Angeles, CA 90095, USA.

E-mail: kmiki@nfri.re.kr

Abstract. Understanding the L→H and H→L transitions is crucial to successful Iter operation. In this paper we present novel theoretical and modelling study results on the *spatio-temporal* dynamics of the transition. We place spatial emphasis on the role of zonal flows and the micro→macro connection between dynamics and the power threshold (P_T) dependencies. The model studied evolves five coupled fields in time and one space dimension, in simplified geometry. The content of this paper is a.) the model fundamentals and the space-time evolution during the L→I→H transition, b.) the physics origin of the well known ∇B-drift asymmetry in P_T, c.) the role of heat avalanches in the intrinsic variability of the L→H transition, d.) the dynamics of the H→L back transition and the physics of hysteresis, e.) conclusion and discussion, with a special emphasis on the implications of transition dynamics for the L→H power threshold scalings.

1. Introduction

Understanding of (low)L→(high)H transition physics is crucial to a successful Iter. Nevertheless, the power requirement for accessing the H-mode or the back transition dynamics from the H to L-mode has been remaining unclear. The L→H power threshold scalings[1, 2] remains only a 'blunt instrument' for progress. Then, it begs the question of can we understand the physics behind the experimental scalings from theory and microphysics experiments?

Recent experiments have revealed the physical mechanism behind the L→H transition from the limit-cycle oscillation(LCO) of E_r interacting with turbulent fluctuations[3]. The pre-transition LCO is also observed in NSTX, ASDEX-Upgrade, EAST etc[4, 5, 6, 7]. The experimental results show limit-cycles in the E_r and turbulence fluctuations in phase space, suggesting a strong similarity to the two predator-one prey model[8]. The predator-prey model describes interacting zonal flow(ZF) and mean flow(MF) shear suppression of turbulence and MF-ZF competition. The model recovers an L→H transition triggered by ZF shearing and a pre-transition limit-cycle oscillation(LCO) due to interplay among turbulence, ZF, and MF. Thus, the experimental observation of the LCO indicates that ZF shearing, i.e. micro-physics, can connect with the macro dynamics of the L→H transition.

With regard to the pre-transition LCO, spatio-temporal structure of this sort has now been identified in DIII-D[6] and TJ-II[9]. A Doppler backscattering system (DBS) has measured local density fluctuation and total $E \times B$ flow, with high spatial and temporal resolution. This measurement has provided a new picture of the I-phase as an evolving flow layer structure of LCO. The LCO structure resembles a propagating wave. To relate these findings to the two predator-one prey hypothesis of ZF trigger and mediation, at least a one space dimension version of the multi-predator-prey model[10] is necessary here. Such a one-dimensional model can predict the *spatio-temporal* evolution of the pedestal through the L→H transition, as well as the spatial structure of the LCO.

In this paper, we present novel theoretical results on the spatio-temporal dynamics of L→H transition, with a special emphasis on the role of zonal flows. The model effectively couples mesoscale evolution of fluctuation intensity ($n \neq 0$) and zonal flow ($n = 0$) shear to transport evolution of profiles and mean shear. The coefficients in this mean field model are determined by the underlying primitive equations. Universality classes for the model coefficients are discussed in Ref. [11].

The remainder of this paper is organized as follows. In Section 2, we introduce the model fundamentals and the space-time evolution during the L→I→H transition. In Section 3, we show the physics origin of the well known ∇B-drift asymmetry in P_T. In Section 4, we discuss the role of heat avalanches in the intrinsic variability of the L→H transition. In Section 5, we introduce the H→L back transition and the physics of hysteresis. In Section 6, we conclude and discuss remaining issues.

2. L→I→H Evolution

We have significantly extended an earlier 2 predator- 1 prey model[8] to develop a 5-field reduced mesoscale (envelope) model which evolves turbulence intensity (I), zonal flow shear ($V'_{\rm ZF}$), ion pressure (p_i), density (n), and mean poloidal mass flow ($\langle v_\theta \rangle$) in radius and time, in a simplified geometry. Free boundary conditions are imposed and SOL coupling is neglected. Mean $\mathbf{E} \times \mathbf{B}$ velocity ($\langle V_E \rangle$) is calculated via radial force balance. The details of this model are given elsewhere[10], so we do not repeat them here. We remark that reduced models are necessary to address the L→H transition problem, since no 'first principles' simulation has successfully confronted this phenomenon.

We have investigated the space-time evolution of the L→H transition using our new model. The model captures the essential physics of ZF and mean flow interaction, turbulence suppression by ZF and MF shearing, and poloidal flow evolution, including that driven by turbulence. We also have elucidated how ZF shearing mediates the transition. These findings are in good agreement with findings from several DBS and probe experiments[6] and point to the crucial role of ZFs in the transition dynamics. The specific results of this study are:

(i) Studies with a slow power ramp reveal an L→H transition via an 'intermediate' I-phase, characterized by a train of nonlinear waves, which, locally, are limit-cycle oscillations (LCOs). These are illustrated in Figs. 1 and 2. The I-phase is initiated near, but not *at* the LCFS. In this model, the mean flow shear peak nucleates at the fixed edge boundary. This result, a consequence of boundary conditions, should be compared with results from DIII-D, where the total $E \times B$ flow velocity negative well nucleates at the edge region and rises to be positive away from the LCFS.

(ii) The I-phase is a multi-predator-prey oscillation of turbulence intensity, zonal flow and mean flow shear. There is a clear threshold to access the I-phase, which is set by zonal flow damping. The LCO at a given radius is seen as a slice through an inward propagating nonlinear wave, which appears as a slowly oscillating region of expanding width, as shown in Fig. 2. Mean flow shear growth begins *after* the onset of I-phase, with a clearly identifiable lag time. Thus the L→I→L loop has finite, though not necessarily strong, hysteresis. MF shear increases during the LCO.

(iii) The LCO period increases approaching the transition (see Fig. 1). Approaching the transition, turbulence peak rises but becomes *shaper* in space and time (see Fig. 2a). This is also observed in a spectrogram from HL-2A experiments[12]. The I-phase terminates abruptly at transition, with rapid growth of mean flow shear. At the transition, edge gradients increase from their I-phase value, and pedestals in density, and temperature begin to expand inward. The width of the I-phase ZF region sets the initial scale of the H-mode pedestal. Local turbulence intensity peaks just prior to transition. Growth of mean flow shear locks in the transition to H-mode.

(iv) The phase delay between turbulence and zonal flow increases from $\pi/2$ to π

during the I-phase, consistent with the model[8] and also DIII-D results[6] (see Fig. 3). The diamagnetic shear oscillates with growing amplitude in I-phase, then increases abruptly at the L→H transition. The growth of the diamagnetic flow shear amplitude occurs only in I-phase, not in L-mode. The peak of the ZF shear increases just prior to transition. This is consistent with analysis of EAST experiments, which indicate that ZF shearing is dominant just prior to the L→H transition[13, 14].

(v) The actual transition event can be abrupt, even if the power ramp and LCO evolve slowly. This picture is consistent with experiments. The pedestal expands *after* the L→H transition.

(vi) Numerical studies reveal that two types of 'transition' occurs sequentially. With a slow power ramp, L→H transition occurs via a transition to I-phase, which clearly manifests a quasi-periodic oscillation. On the other hand, during a fast power ramp, the I-phase is compressed into a single burst of ZF, leading to a transition without an LCO, as shown in Fig. 4. Here how *fast* the ramp must be so as to prevent an LCO depends on the ramp rate, as compared to the period of the limit-cycle. These features resemble that observed in TJ-II, shown in Fig. 7 of Ref. [15].

As shown in Fig. 5, studies of power threshold with various ZF damping and neoclassical poloidal viscosity indicate that *larger neutral CX increases the power threshold.* More generally, increasing ZF damping increases the power threshold, suggesting that ZF is fundamental to the transition. During the evolution of the ZF acts as 'holding pattern', in which to store large fluctuation energy *without increasing transport*, (since $n = 0$ for ZF), thus allowing the mean flow shear to grow as profiles steepen. Mean flow shear, however, ultimately is required to 'lock in' the state of quenched turbulence. Without mean shear growth, the LCO of I-phase will persist indefinitely. Therefore the ZF damping should enter the power threshold condition, but does not exclusively determine it. At least, the trend that stronger ZF damping $\gamma_{\rm damp}$ raises the power threshold P_T is relevant to the empirical scaling in the higher density region, because $\gamma_{\rm damp} \propto \nu_{ii} \propto n$. More systematic and quantitative study of the power threshold requires modification of mean flow evolution by SOL-edge interaction, as discussed in Section 3.

These results also suggest implications for future steady state experiments. We note that neutral CX can damp zonal flows in experiments[16], indicating that high edge neutral density is unfavorable to transition, as shown in Fig. 5. This finding can be related to the long established experimental lore concerning the power threshold, 'dirty machines', re-cycling, etc. The results have implication for the recovery of H-mode in steady state operation, should it be lost. In such a case, wall saturation and consequent increased re-cycling can ultimately lead to strong CX damping of ZFs, making it difficult to recover the H-mode, should a back-transition occur. This suggests that proper wall conditioning, or reduction of wall impurity saturation, is necessary throughout the long pulse H-mode operation, because the ZF shearing necessary to trigger the transition may be more difficult to achieve.

3. Physics of the ∇B-Drift Asymmetry.

One of the most persistent puzzles in L→H transition phenomenology is why power threshold are lower for lower-single-null (LSN) configurations (with ∇B drift *into* the X-point) than for upper-single-null (USN) configurations (with ∇B-drift *away* from the X-point). Here, we briefly summarize recent progress on a model which links this asymmetry to the interplay of magnetic shear and $E \times B$ shear induced eddy tilting and its affection on Reynolds stress generated $E \times B$ flows[17].

Simply put, either magnetic or electric field shear acts to tilt eddies. Thus, the *local* radial wave number is given by,

$$k_r(\theta) = k_r(\theta_0) + [(\theta - \theta_0)\hat{s} - V_E'\tau_c]k_\theta \tag{1}$$

where the first term is due to magnetic shear tilting, which varies with angle θ, and the second term is $E \times B$ shear tilting, which grows in time. Hereafter, we take $\tau = \tau_c$, the correlation time and thus the eddy life time and $\theta_0 = 0$. Given the structure of $k_r(\theta)$, the total non-diffusive (i.e. 'residual') Reynolds stress is

$$\langle \tilde{v_r}\tilde{v_\theta} \rangle = \langle \tilde{v_r}^2(0) \rangle F^2(\theta)[-\theta\hat{s} + V_E'\tau_c] \tag{2}$$

The θ-dependence of eddy tilting is shown in Fig. (6). Now the 'point' is readily apparent from observing that $\langle \theta F^2(\theta) \rangle_\theta$ will trend to vanish unless there is an imbalance between contributions to the flux surface average from $\theta > 0$ and $\theta < 0$ – i.e. an up-down asymmetry, as for LSN vs USN! The remaining question is to determine *when the magnetic shear induced stress adds or subtracts to the* $\mathbf{E} \times \mathbf{B}$ *shear induced stress and the related flow production.* To do that, the electric field shear must be computed self-consistently, by solving the poloidal momentum balance equation:

$$\partial_t \langle v_\theta \rangle + \partial_r \langle \tilde{v_r}\tilde{v_\theta} \rangle = -\gamma_{CX} \langle v_\theta \rangle \tag{3}$$

where

$$\langle \tilde{v_r}\tilde{v_\theta} \rangle = -\chi_\theta \partial_r \langle v_\theta \rangle + \Pi_{\hat{s}} + \Pi_{V_E'} \tag{4}$$

so

$$\partial_t v_\theta + \partial_r(\Pi_{\hat{s}} + \Pi_{V_E'}) = -(\gamma_{CX} - \partial_r \chi_\theta \partial_r)[V_E + V_{*i}]. \tag{5}$$

Here we have used radial force balance while neglecting toroidal flow, have accounted for turbulent viscosity (χ_θ) and frictional damping (γ_{CX}) and retained magnetic shear ($\Pi_{\hat{s}}$) and electric field shear ($\Pi_{V_E'}$) driven residual stresses. Of course, $\langle V_E \rangle'$ in the latter also must satisfy radial force balance. Equation (5) is solved while imposing the boundary conditions $E_r = -3\partial_r T_e$ (i.e. determined by SOL physics) at the LCFS and $V_E = -V_{*i}$ in the core. Assuming gyro-Bohm (GB) turbulence and using standard parameters, we calculate V_E/c_s and V_E', as shown in Fig. 7. It is readily apparent that favorable (i.e. LSN) configurations give a larger and stronger edge electric field shear layer than do unfavorable (i.e. USN) configurations. The effect is significant – maximum shears are twice as strong for LSN than for USN. The corresponding Reynolds

force is plotted in Fig. (8). We also note that the effect is not poloidal symmetric, when variation in θ is considered. Thus, the flux surface averaged Reynolds stress cannot be inferred from a single point measurement.

Future work will aim to integrate this analysis into the model discussed in Section 2. Along the way, the treatment of the SOL boundary conditions will be generalized.

4. Intrinsic Variability, Heat Avalanches, and Noisey Transitions

It is well known that the L→H transition exhibits significant variability. The scatter in P_T trends is large. Also, many anecdotes exist describing sudden transitions in stationary, slightly subcritical states. In particular, I-phase→H-phase transition appear noisey and unpredictable. Many observations have been reported, which describe prolonged (i.e. $>$ 100msec) I-phases at constant $P_{\rm in}$, followed by sudden L→H transitions. All this suggests that variability exists, and may be both *extrinsic*, induced by the control system, heating, etc. system noise, and *intrinsic*, induced by the stochastic character of the plasma dynamics. Intrinsic variability can impact the transition via noise, as suggested some time ago[18], but not pursued since. Here we argue that *edge heat flux variability* is a prime candidate for the origin of intrinsic noise in the L→H transition. Such intrinsic variability associated with heat flux fluctuations is relevant to the L→H transition in Iter, which will operate close to threshold.

The classic example of the effects of variability in the heat flux is the well known observation that, for $P_{\rm in} \leq P_T$, a sufficiently large sawtooth heat pulse can trigger a transition upon its arrival at the LCFS[19]. This demonstrates the sensitivity of the transition to the (local) *surface heat flux*, and not (global) power. More recently, studies of edge turbulence on EAST have noted that sawtooth heat pulses coherently modulate measured edge Reynolds stresses $\langle \tilde{v_r}\tilde{v_\theta}\rangle$ and zonal flows, thus establishing the macro→micro connection[7]. Interestingly though, in addition to the familiar coherent response, the EAST studies observed *stochastic, high frequency modulations*, suggestive of an ensemble of 'micro-pulses'. Consistent with this, EAST results also indicated that significant negative stochastic spikes in E_r occur. This 'stochastic spiking' is suggestive of the 'noisey transition' hypothesis, in turn begging the question of what is the physical origin of the spikes? An obvious and likely candidate is *heat avalanching*. Heat transport (and turbulence) is flux driven, so local gradients adjust to match the heat flux. This leads to interaction of adjacent cells or eddies to form *avalanches*, as in sand pile SOC models[20]. Avalanches are finite life time 'transport events', with a scale $l_{\rm aval} > \Delta r$, the turbulent correlation length. Symptoms of avalanching are the appearance of a $1/f$ spectrum in the heat flux fluctuations and a non-Gaussian tail of the heat flux PDF[21]. Avalanches have been observed in many simulations of transport and micro-turbulence[22, 23]. These considerations suggest that the edge is continuously bombarded by an ensemble of micro heat pulses which are due to the nature of flux-driven turbulence. Such avalanches are a natural source of intrinsic variability.

There are many obvious questions concerning the effects of avalanching. Does heat

flux noise trigger subcritical transitions, where "subcritical" $\equiv \langle Q\rangle - Q_{\rm crit} < 0$? Here $Q_{\rm crit}$ is the critical surface heat flux for transition, and corresponds to P_T. Does the nature of the noise matter – i.e. is subcritical transition attained more easily? Is there a clear trend in whether or not the transition is achieved as one explores the space of heat flux variance (σ^2) vs. deviation from threshold $(Q_{\rm crit} - \langle Q\rangle)/Q_{\rm crit}$. More fundamentally, what is the most meaningful formulation of the stochastic transition problem? To address these questions with our model, we observe that the model is local and diffusive albeit flux driven. In particular, intensity evolution and heat balance give $\partial_t I = \gamma(R/L_T - R/L_{Tc}, \cdots)I$ and $Q = -n(\chi_{\rm turb} + \chi_{\rm neo})\nabla T$, respectively. Thus, the fluctuation(including ZF) source $\gamma I \simeq (\gamma_0/nT) f_T I Q/(\chi_{\rm turb} + \chi_{\rm neo})$. Here f_T is a threshold function, which introduces strong nonlinearity near threshold. Noting that $\chi_{\rm turb} \sim \chi_0 I$, it follows that $\gamma I \sim (\gamma_0/nT) f_T I Q/\chi_{\rm neo}$ close to threshold and $\sim (\gamma_0/nT\chi_0)Q$ above threshold. As the pre-transition edge is strongly turbulent, we see that fluctuation energy directly tracks the heat flux in the regime of interest. To model the intrinsic variability of avalanching, we introduce a fluctuating component to the heat flux, so now $Q = \langle Q\rangle + \tilde{Q}(t)$. The frequency spectrum of $\tilde{Q}$ is adjustable, i.e. $\langle \tilde{Q}^2\rangle_\omega \sim \omega^{-\alpha}, \alpha = 0, 1, 2, \cdots$ so as to model states of white noise ($\alpha = 0$), avalanching ($\alpha = 1$), diffusive transport ($\alpha = 2$) etc.

Results of model studies confirm that heat flux variability indeed can induce subcritical transitions. Fig. 9a shows a stationary I-phase, at subcritical $\langle Q\rangle$. Adding white noise results in a subcritical transition, after a time delay, as shown in Fig. 9b. Interestingly, adding much weaker *noise with a* $1/f$ frequency spectrum results in a subcritical transition after a slightly long time delay. Fig. 10 confirms the result that subcritical transitions occur more easily for $1/f$ than for white noise of equal net intensity. We speculate this is because $1/f$ noise has more power at lower frequencies, with stronger autocorrelation, which facilitates stronger and more prolonged feedback. This hypothesis is supported by Fig. 10 which shows plots of noise intensity vs. $Q_{\rm crit} - \langle Q\rangle$ for white (a.), $1/f$ (b.), and $1/f^2$ (c.) noise. Note the model difference between the domains of transition in Figs. 10a and 10b, while the results of Figs. 10b and 10c are rather similar. This points to the key role of low frequency heat flux variabilities in the transition.

To conclude this section, we remark on the lessons for experimentalists which it conveys. First, to assess intrinsic variability, it is essential to characterize heat avalanche, and turbulence spreading, especially near the edge (i.e. from No Man's Land to the LCFS). DBS and ECEI are natural candidates. Second, given that avalanches occurs on mesoscale $l_{\rm mess} > \Delta_c$, it would be useful to determine the thickness of the influence layer around the LCFS. By influence layer, we mean the zone from which perturbations which trigger the transition may originate. Finally, fast externally driven modulation experiments, and perhaps stochastic modulation experiments, would be of great interest.

5. H→L Back Transitions and the Physics of Hysteresis

There is growing interest in H→L back transitions, since Iter will operate close to threshold ($P \sim P_T$), with limited control ($\langle\tau_{\rm resp}\rangle > \tau_E$, where $\tau_{\rm resp}$ is the response time of the control system). Thus, H→L transition dynamics and the understanding of hysteresis are critical. Hysteresis also gives a fundamental clue as to the 'order' of the transition. Some of the major questions concerning H→L back transition dynamics are:

(i) What is the fundamental process of the back transition? Is there a feedback loop?

(ii) does the plasma re-visit I-phase in the course of the back transition? Doing so would ensure a 'soft landing' after the back transition – an outcome which clearly is desirable;

(iii) How do we describe and quantify hysteresis? How do profiles affect hysteresis? Which transport channel exhibits the shortest hysteresis?

Here, we use our model to investigate these questions. We focus on an idealized model of ELM-free back transition dynamics – i.e. a scenario of a ramp down from $P > P_{\rm crit}$. This allows us to separate transport from MHD and ELM physics. Similar physical experiments would be enlightening!

First, regarding the fundamental nature, of the back transition, Fig. 11 shows quite clearly that in at least this case it is fundamentally a process of turbulence spreading into a quiescent region. Figure 11 shows the advance of the turbulent core into the pedestal (c.f. the evolution of the dashed blue curve). It also shows the drop in the mean shear (red curve), as the region of maximal flow curvature – the 'corner', where the turbulent core connects to the steep gradient pedestal – collapses toward the LCFS. Finally, we see that the ZF intensity (green curve) is dragged along by the turbulence, as it must be. Thus, we see that the back transition is indeed a process where by the interface between the turbulent core and the quiescent or neoclassical pedestal advances toward the boundary. This turbulence spreading process is regulated by nonlinear couplings (i.e. D_0), zonal and mean flow control parameters (i.e. damping) and the transport coefficient which determine the mean flow shear.

As feedback loop structure, since turbulence spreading is the key process, it's apparent that the feedback mechanism is: a drop in heat flux $Q \rightarrow$ a decrease in $\langle v_E\rangle'^2 \rightarrow$invasion of the quiescent zone by turbulence $\rightarrow$an increase in transport $\rightarrow$a drop in $\nabla T \rightarrow$a decrease in $\langle v_E\rangle'^2$, etc. Two key open questions here are: i.) how much spreading can the pedestal tolerate before complete collapse?, ii.) does the threshold power for back transition $P_{\rm TB}$ correspond to that for which the spreading front penetrate the LCFS. There questions will be answered in a future paper.

Second, regarding the question of the *dynamics* of H→L back transition, recent cases from DBS studies on DIII-D[24, 25] suggest that the answer is 'yes!' – the system *does* pass through the I-phase during the H→L back transition. Indeed, the LCO behavior seen in the forward transition is mirrored in the back transition, with the ZF oscillation frequency *increasing* as the back transition progresses and relative

physics between fluctuation and $E \times B$ velocity evolving the same way. Of course, the ZF velocity peaks at the beginning of the back I-phase, but then decreases.

We emphasize, though, the key that in the back transition, the LCO *is nucleated at the pedestal shoulder*, since that is the site of residual turbulence in H-mode. This is related to the fundamental character of the back transition, which is a process of turbulence penetration from an active core into the quiescent pedestal. The results of model studies are shown in Fig. 12a,b,c. Figure 12b shows a slower ramp down than Fig. 12a, while Fig. 12b shows a faster ramp down. Figure 12c shows clearly that an I-phase and LCO appear on route from H-mode to L-mode. Note here, though, that the LCO frequency *increases* during the back I-phase, and the zone of ZF and turbulence activity slowly expands toward the LCFS. As before, the LCO induces ∇p oscillations which drive D_α bursts. These, then, may correspond to their so called 'Type-III ELMs' reported during the back transition[26].

Figure 12b examines the same case, with a 5 times slower ramp-down. Results are similar, with a more extended I-phase. Fig. 12c shows a 10 times faster ramp down. There, only a single burst of ZF activity occurs. The collapse to L-mode proceeds quickly. Thus, it seems that the landing will not always be 'soft', as the duration of I-phase in the back transition depends upon the ramp down rate.

Turning to the critically important question of hysteresis, we note that this question is both i.) highly relevant to Iter, ii.) fundamental to the nature of the bifurcation transition, and thus of great interest. However, it's curious to note that in distinct contrast to the plethora of papers on L→H dynamics and the extensive databases for threshold power, there are very few, if any, dedicated studies of back transition and no databases for hysteresis. Indeed, a fundamental question hysteresis is *how to quantify it, in terms of physical quantities*, other than the global $P_{\mathrm{L}\to\mathrm{H}}/P_{\mathrm{H}\to\mathrm{L}}$ (a holdover from the days of global scaling). Of course, we realize that the physical underpinning of hysteresis phenomena is the difference in transport between the L (strongly turbulent) and H (neoclassical/weakly turbulent) regions. However, the questions of which channel?, what quantity? etc. remain unanswered. Here, we define hysteresis in a transported quantity as the ratio of the H-mode pedestal inverse scale length of that quantity to its pre-transition counterpart, i.e. $1/L_{A,\mathrm{per}}/1/L_{\mathrm{A,L}} = L_{A,\mathrm{L}}/L_{A,\mathrm{per}}$. This in turn suggests that the corresponding Nusselt number $\mathrm{Nu}_A = D_{A,L}/D_{A,ped}$ is the natural parameter with which to describe hysteresis. Note that $D_{A,ped}$ is the *effective* pedestal diffusivity. In the case of T_i, $D_{T_i,ped} = \chi_{i,neo}$ but for density $D_{n,ped} = D_{n,resid}$, the residual turbulent transport in H-mode. Note then that we expect hysteresis to be *relative*, i.e. some gradients will relax faster than others. Relative hysteresis is naturally described by pedestal or residual Prandtl number $\mathrm{Pr}_{ped} \equiv D_{n,ped}/\chi_{i,ped}$ etc. Thus, relative hysteresis between density and temperature, should appear as a finite area loop in the phase portrait of $1/L_n$ vs $1/L_{T_i}$, with area scaling inversely with Pr_{resid}.

Model studies of hysteresis in scale lengths L_n, L_p and quantities n, p have been carried out. The studies are straightforward (i.e. ramps up, then down) and net hysteresis is calculated by measurement of the area of the hysteresis loop at $r/a = .95$.

Figure 13a *shows that measured hysteresis indeed tracks Nusselt number*, which varies as $(\chi_{\rm i,neo,0}/\chi_{\rm i,neo})$. Here $\chi_{\rm i,ped} \sim D_{\rm n,ped} \sim \chi_{\rm i,neo}$, through $D_{\rm n,ped}$ and $\chi_{\rm i,neo}$ differ by a numerical factor. $\chi_{\rm i,neo,0}$ is a normalizing factor. The evident deviation from linear proportionality of hysteresis to Nu at large Nu is likely due to difficulties in accurate measurement of loop area. Figures 13b,c show the *relative* hysteresis of $1/L_n$ and $1/L_T$, for two different values of ${\rm Pr}_{\rm ped} \equiv D_{\rm n,ped}/\chi_{\rm i,neo}$. Relative hysteresis is evident, and increases with $1/{\rm Pr}_{\rm ped}$, as it should. Finite relative hysteresis implies that the H→L relaxation dynamics will not be the same in all quantities. Fig. 14a,b shows hysteresis loop in *scale lengths* $1/L_p$ and $1/L_n$ vs heat flux Q, while Fig. 14c,d shows the corresponding loops for *quantities* p, n. Interestingly, *the gradient scale lengths hysteresis plots are different from the quantity hysteresis plots*. The former have a (crudely) rectangular shape while the latter one rather clearly triangular. Of course, there is no a-priori reason to expect these two sets of figures to be equivalent. This observation illustrates the need to identify the most physically relevant quantities in terms of which to define hysteresis.

Finally, we explore the macro-micro connection in Fig. (15). The dependence of ZF damping on ion collisionality is equivalent to a dependence on $\chi_{\rm i,neo}$. Thus for equal ramp down rates, there should be a relation between $\chi_{\rm i,neo}$ and back-I phase LCO frequency. This is confirmed in Fig. (15), which shows higher LCO frequency for longer $\chi_{\rm i,neo}$ (indicative of smaller Nu.

We now summarize this discussion of hysteresis and discuss its implication for experiment. Model studies indicate

(i) hysteresis in lengh scale tracks Nu, as expected. Further study of hysteresis near criticality is required.

(ii) relative hysteresis appears, and is related to ${\rm Pr}_{\rm ped}$. Thus, we expect the H-mode to be more resilient in L_n^{-1} than in $L_{T_i}^{-1}$.

(iii) different quantities $(T, L_T^{-1}, \cdots)$ exhibit different hysteresis behavior. Scale length hysteresis seem more fundamental than quantity hysteresis, as scale length are more directly linked to the driving flux.

(iv) hysteresis appears linked to pedestal profile structure, since the back transition develops from the pedestal shoulder.

Some of the implications for experiment are:

(i) study of ELM-free back transitions are illuminating, so as to isolate transport physics from MHD physics.

(ii) fluctuation studies during the back transition should track the turbulence invasion front, and attempt to determine the lag, if any, between changes in v_E and changes in intensity.

(iii) regarding the important subject of hysteresis,

- hysteresis should be characterized in terms of *local* physical quantities. Studies of scale length vs. Nu would be especially illuminating.

- relative hysteresis studies of $1/L_{T_i}$ vs $1/L_n$ and $1/L_{T_i}$ vs $1/L_{V_\phi}$ would be interesting, both on their own account and for their implications concern in, pedestal transport.
- I-phase dynamics should be studied in connection with hysteresis.

We conclude this section with the observation that back transition dynamics is an *ideal* testing ground for this or any other model. This is because the lack of data and experience on back transitions necessarily forces the model to function in predictive, rather than explanatory, mode. Predictive tests of models against back transition 'stress tests' should be pursued.

6. Conclusion – toward the Power Threshold.

We conclude by commenting on the 'bottom line' question in L→H transition physics, namely the power threshold. It is now rather clear that $P_T(n)$ follows a curve with a minimum[2], as sketched in Fig. 16. For low n, $P_T(n)$ decreases, reaches a minimum and then increases with n, roughly, linearly. From our understanding of L→H transition dynamics (i.e. this model), we know that:

(i) the ZF 'triggers' the transition;

(ii) the L→H transition is '2 step' : L→I and I→H;

(iii) at higher density, the two steps are not distinguishable without detailed analysis;

(iv) zonal flow damping is proportional to $\nu_{ii}+\nu_{\rm CX}$ and thus density and neutral density.

Of course, the two steps are severely compressed by a fast power ramp. In that case, the I-phase is just a short burst of ZF activity.

Thus, the model discussed here captures the essential physics of P_T in the high n branch. Interestingly, though:

- at low density, where $P_T(n)$ drops with n, a window for an identifiable and distinct I-phase range opens;
- the lower P_T bound of that window – namely $P_{\rm crit}$ to access *I-phase* – falls roughly on the low n extrapolation of the high n linear proportionality, which seems related to zonal flow damping.

Thus, *it seems that ZF damping continues to control access to I-phase at low density, but additional physics enters the I→H transition in that regime.* At high density, L→I and I→H are macroscopically indistinguishable. Noting that low density is where electron-ion decoupling occurs, we speculate that the low density I→H threshold may be addressed by this model via:

(i) separately evolving T_e and T_i including coupling and boundary conditions;

(ii) adopting Fundamenski *et al.*'s approach to linking $T_{e,LCFS}$ to divertor heat transport[27]. This seems quite relevant at low density.

Success here would recover the basic structure of the $P_T(n)$ curve in the context of a model which already successfully captures the dynamics of the L→I→H transition. Work is ongoing.

Acknowledgement

The authors acknowledge stimulating discussions with S.H. Hahn, T.S. Hahm, Z. Yan, H. Jhang, C. Hidalgo, G. McKee, M. Xu, and A. Hubbard. This work was supported by the WCI Program of the National Research Foundation of Korea funded by the Ministry of Education, Science and Technology of Korea [WCI 2009-001] and the Department of Energy under Award Number DE-FG02-04ER54738 and CMTFO.

References

[1] MARTIN, Y. R., TAKIZUKA, T., and THE ITPA CDBM H-MODE THRESHOLD DATABASE WORKING GROUP, Journal of Physics: Conference Series **123** (2008) 012033.
[2] RYTER, F., PÜTTERICH, T., REICH, M., et al., Nuclear Fusion **49** (2009) 062003.
[3] ESTRADA, T., HAPPEL, T., HIDALGO, C., ASCASIBAR, E., and BLANCO, E., EPL **92** (2010) 35001.
[4] ZWEBEN, S. J., MAQUEDA, R. J., HAGER, R., et al., Phys. Plasmas **17** (2010) 102502.
[5] CONWAY, G. D., ANGIONI, C., RYTER, F., SAUTER, P., and VICENTE, J., Phys. Rev. Lett. **106** (2011) 065001.
[6] SCHMITZ, L., ZENG, L., RHODES, T. L., et al., Phys. Rev. Lett. **108** (2012) 155002.
[7] XU, G. S., WAN, B. N., WANG, H. Q., et al., Phys. Rev. Lett. **107** (2011) 125001.
[8] KIM, E.-J. and DIAMOND, P. H., Phys. Rev. Lett. **90** (2003) 185006.
[9] ESTRADA, T., HIDALGO, C., HAPPEL, T., and DIAMOND, P. H., Phys. Rev. Lett. **107** (2011) 245004.
[10] MIKI, K., DIAMOND, P. H., GURCAN, O. D., et al., Physics of Plasmas **19** (2012) 092306.
[11] DIAMOND, P. H., LIANG, Y. M., CARRERAS, B. A., and TERRY, P. W., Phys. Rev. Lett. **72** (1994) 2565.
[12] ZHAO, K. et al., in *Proceedings of the 24th IAEA Fusion Energy Conf. (San Diego, USA)*, pp. IAEA–CN–197/EX/7–2Ra, 2012.
[13] MANZ, P., XU, G. S., WAN, B. N., et al., Physics of Plasmas **19** (2012) 072311.
[14] TYNAN, G. et al., in *Proceedings of the 24th IAEA Fusion Energy Conf. (San Diego, USA)*, pp. IAEA–CN–197/EX/10–3, 2012.
[15] ESTRADA, T., HAPPEL, T., ELISEEV, L., et al., Plasma Physics and Controlled Fusion **51** (2009) 124015.
[16] XU, Y., CARRALERO, D., HIDALGO, C., et al., Nuclear Fusion **51** (2011) 063020.
[17] FEDORCZAK, N., DIAMOND, P., TYNAN, G., and MANZ, P., Nuclear Fusion **52** (2012) 103013.
[18] ITOH, S.-I., ITOH, K., and TODA, S., Plasma Phys. Control. Fusion **45** (2003) 823.
[19] WAGNER, F., FUSSMANN, G., GRAVE, T., et al., Phys. Rev. Lett. **53** (1984) 1453.
[20] HWA, T. and KARDAR, M., Phys. Rev. A **45** (1992) 7002.
[21] TOKUNAGA, S., JHANG, H., KIM, S. S., and DIAMOND, P. H., Physics of Plasmas **19** (2012) 092303.
[22] CARRERAS, B. A., DIAMOND, P. H., and VETOULIS, G., Physics of Plasmas **3** (1996) 4106.
[23] SARAZIN, Y., GRANDGIRARD, V., ABITEBOUL, J., et al., Nuclear Fusion **50** (2010) 054004.
[24] SCHMITZ, L., ZENG, L., RHODES, T. L., et al., in *39th EPS Conference and 16th Int. Congress on Plasma Physics*, 2012.

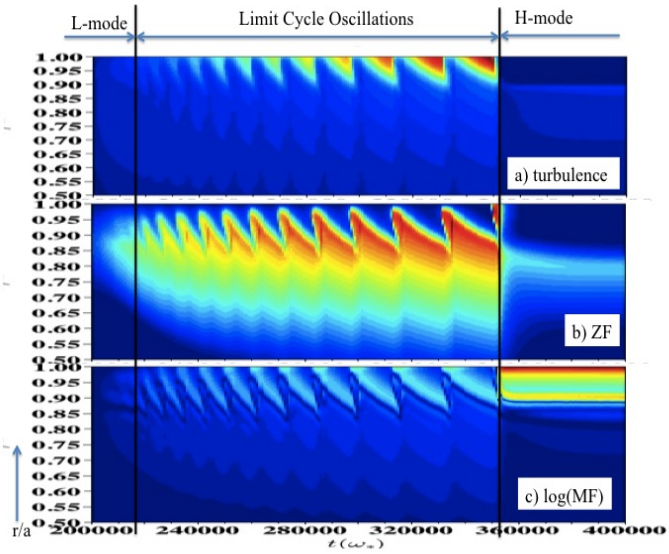

Figure 1. Spatio–temporal evolution of turbulence intensity (a) I, (b) ZF shearing energy E_0, and (c) logarithm of MF shearing energy $\ln(E_V)$ as functions of time t during a power ramp ($2 \times 10^5 < t < 4 \times 10^5$) and as a function of radius ($0.5 < r/a < 1.0$).

[25] SCHMITZ, L. et al., in *Proceedings of the 24th IAEA Fusion Energy Conf. (San Diego, USA)*, pp. IAEA–CN–197/EX/P7–17, 2012.
[26] MCDONALD, D., private communication.
[27] FUNDAMENSKI, W., MILITELLO, F., MOULTON, D., and MCDONALD, D., Nuclear Fusion **52** (2012) 062003.

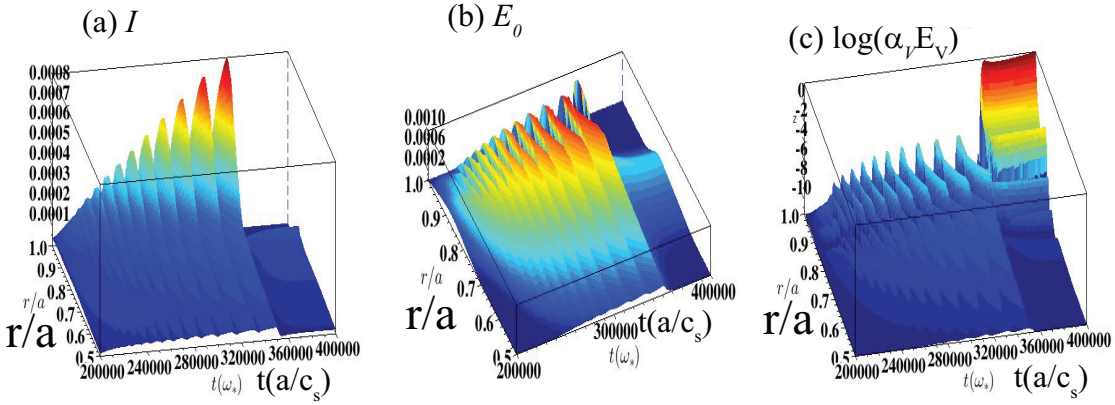

Figure 2. three-dimensional color maps of the time evolution of (a) turbulence intensity I, (b) ZF energy E_0, and (c) MF shearing energy $\ln(E_V)$ as functions of time t (during the slow power ramp regime ($2 \times 10^5 < t < 4 \times 10^5$)) and radius ($0.5 < r/a < 1.0$). These pictures show nonlinear waves propagating inward from the edge layer as the transition develops. What locally appears as a limit cycle is actually a slice of propagating nonlinear wave in the edge layer.

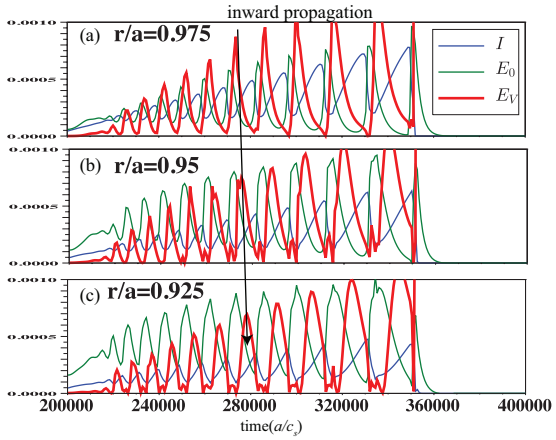

Figure 3. Time evolution of turbulence intensity I(blue solid line), ZF energy E_0 (green solid lines) and mean square MF shear E_V (red bold lines) at various radial location of (a) $r/a = 0.975$, (b) $r/a = 0.950$, and (c) $r/a = 0.925$. The arrow indicates inward propagation of the mean flow peaks. At constant phase, the innermost radius leads in time, suggesting inward propagation.

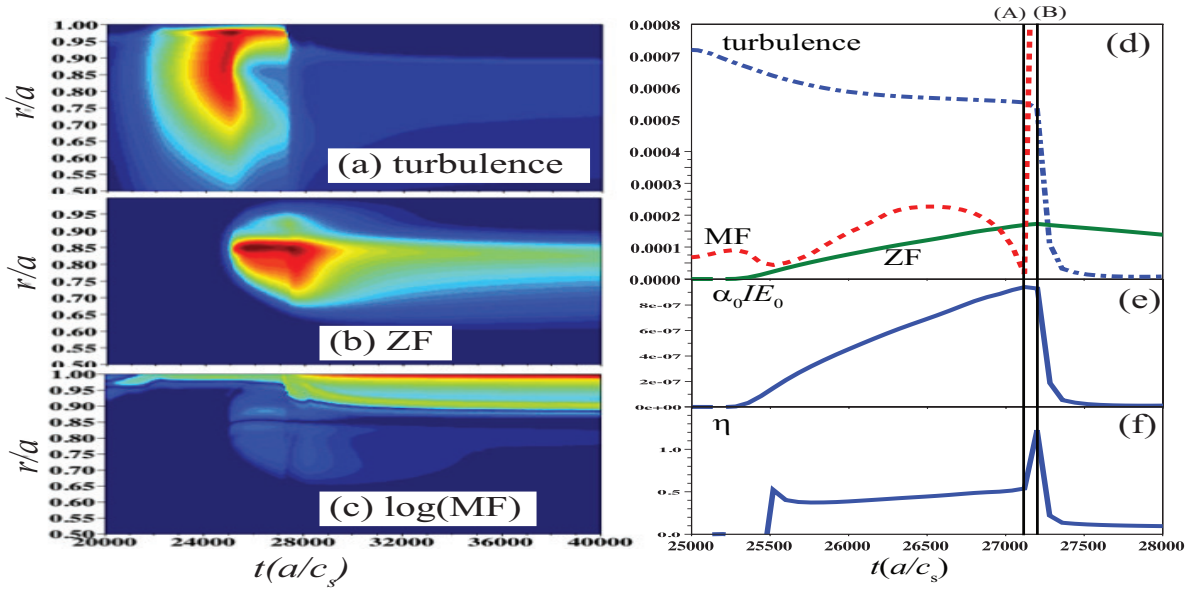

Figure 4. Spatio-temporal evolution of turbulence (a) I, (b) E_0, and (c) $\ln(E_V)$ as a function of time t during a fast power ramp $2 \times 10^4(a/c_s) < t < 4 \times 10^4(a/c_s)$, and radius ($0.5 < r/a < 1.0$). (d) Time evolution of turbulence intensity I (blue chain line), ZF energy E_0 (green solid line), and MF shearing energy E_V (red dotted line). This figure shows that at the L→H transition $t = 2.72 \times 10^4(a/c_s)$, the turbulence quenches at a faster rate, the ZF increases before the transition and damps after the transition, and MF shear rapidly increases at and just after the transition. (e) The evolution of the product quantity $\mathcal{P}_\perp = \alpha I E_0$. The product quantity exhibits a peak just before the transition and quenches after the transition. (f) An evolution of η, showing a single burst at $t = 2.72 \times 10^4(a/c_s)$.

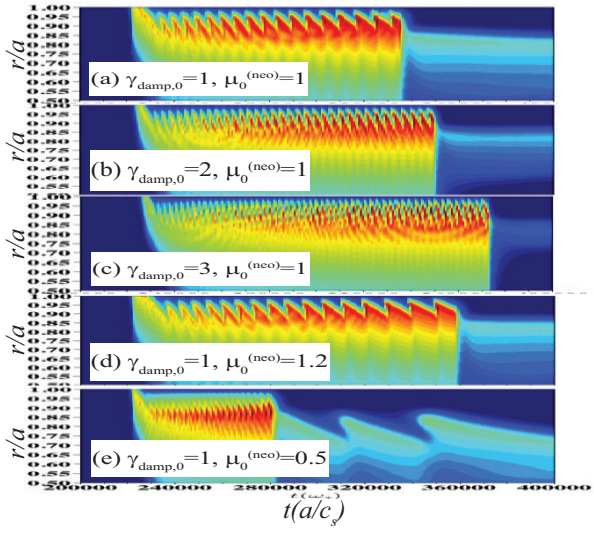

Figure 5. *Spatio-temporal evolution of ZF energy E_0 in cases with a fixed slow heat flux power ramp and various ZF dampings.*

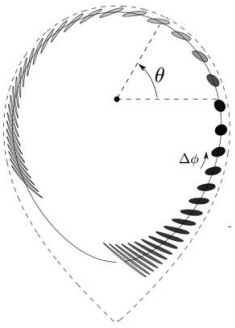

Figure 6. Poloidal cross section of a LSN shaped plasma. The magnetic shear effect is noticeable over the whole surface, and the flux expansion close to the X-point.

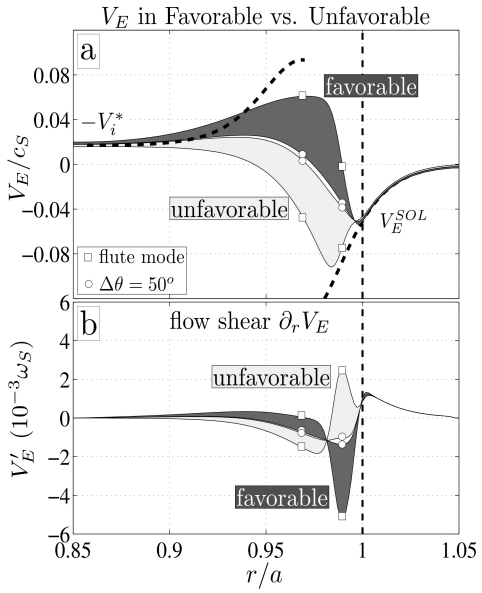

Figure 7. (a) Radial profile of electrostatic velocity for unfavourable (light gray) and favourable (dark grey) configurations. (b) Associated electric shear.

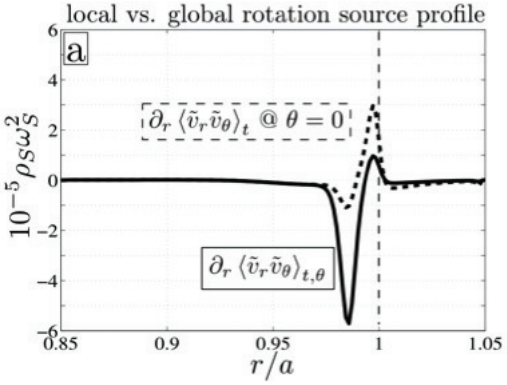

Figure 8. Radial derivative of the Reynolds stress across the profile for a favourable configuration with a ballooning envelope, averaged over the flux surface (full curve) or taken locally at the outboard midplane (dashed line).

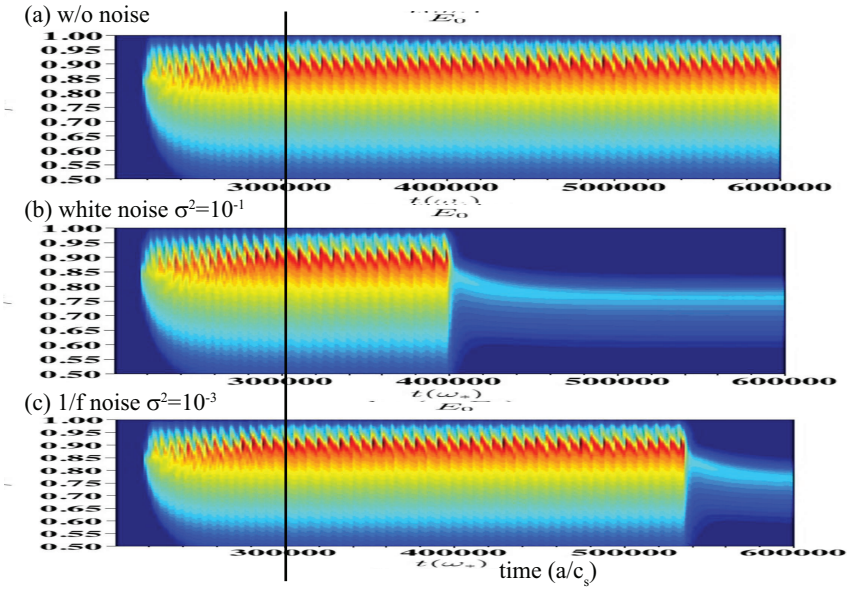

Figure 9. Spatio-temporal evolution of ZF energy with increasing heat flux during $(2.0 < t < 3.0) \times 10^5 (a/c_s)$ to just below the L→H power threshold, and keeping in $t > 3.0 \times 10^5 (a/c_s)$, for the cases (a) without noise, (b) with white noise ($\sigma^2 = 10^{-1}$), and (c) with $1/f$ noise ($\sigma^2 = 10^{-3}$).

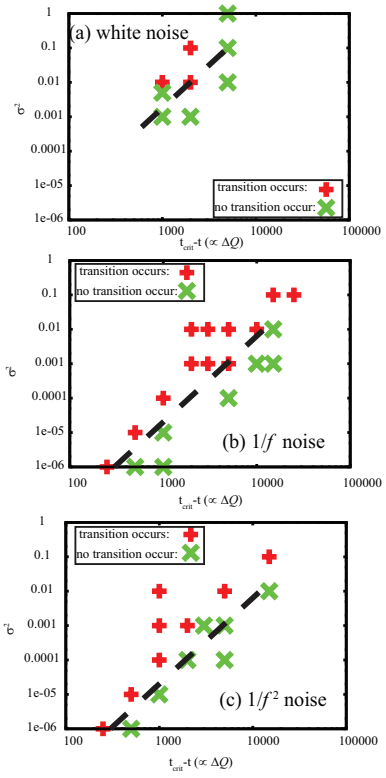

Figure 10. Scan of transition onsets with noise intensity (σ^2) vs different subcriticality (ΔQ), and with different noise colors: (a) white, (b) $1/f$, and (c) $1/f^2$ noises.

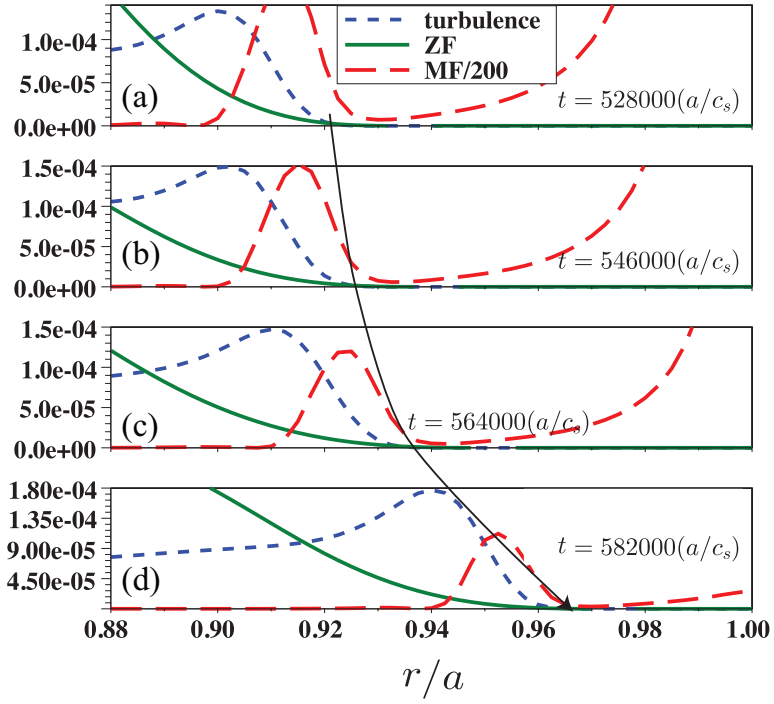

Figure 11. Profiles of turbulence intensity, zonal flow energy, and mean flow shearing energy as a function of radious r/a, with time interval $\Delta t = 1800(a/c_s)$ from (a) through (d).

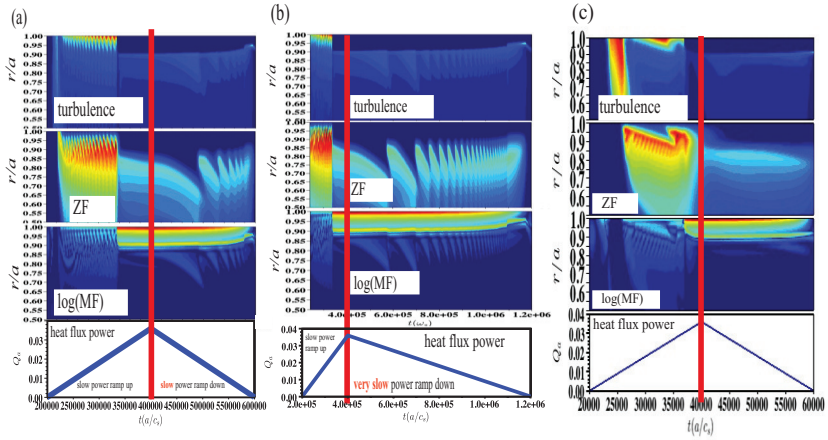

Figure 12. Spatio-temporal evolution of turbulence, zonal flow energy, mean flow, and heat flux, in cases with (a) a ramp at a reference speed, (b) 5 times slower ramp-down speed, and (c) 10 times faster ramp.

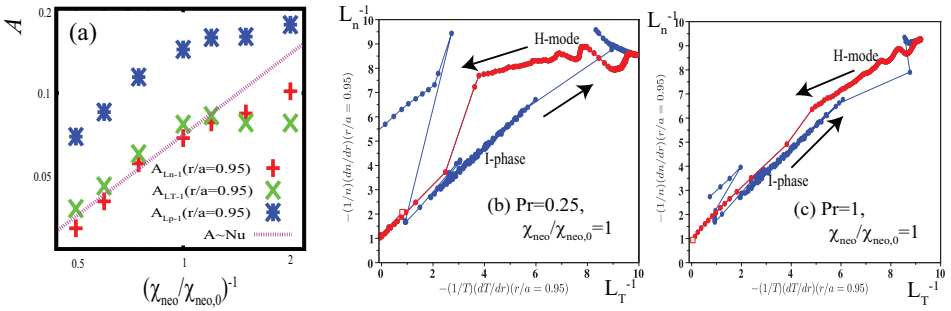

Figure 13. (a) Plots of the area of hysteresis in L_p^{-1}, L_n^{-1}, and L_T^{-1}, compared with the scaling of $A \sim \mathrm{Nu}$. (b,c) Relative hystereses, plots of L_T^{-1} vs L_n^{-1} with (b)$\mathrm{Pr_{neo}} = 0.25$ and (c) $\mathrm{Pr_{neo}} = 1$, exhibiting less strength of relative hysteresis in larger $\mathrm{Pr_{neo}}$.

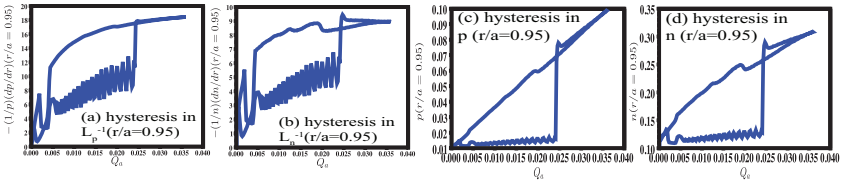

Figure 14. Hystereses with plotting heat flux intensity Q_a vs (a) L_p^{-1}, (b) L_n^{-1}, (c) L_T^{-1}, (d) p, (e) n, and (f) T.

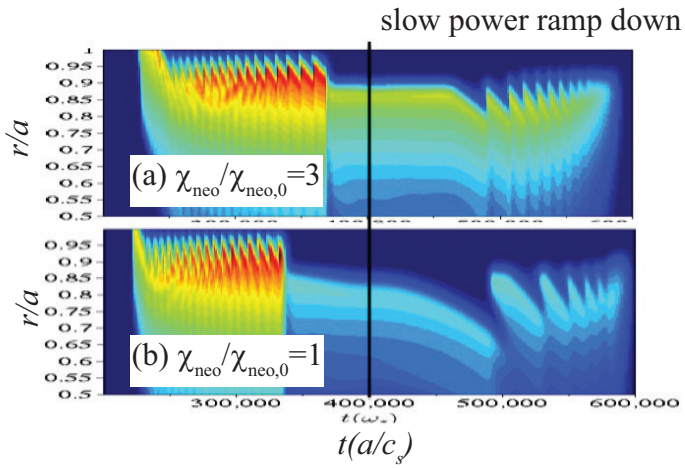

Figure 15. Spatio-temporal evolution of zonal flow energy, with different neoclassical heat diffusivity χ_{neo}

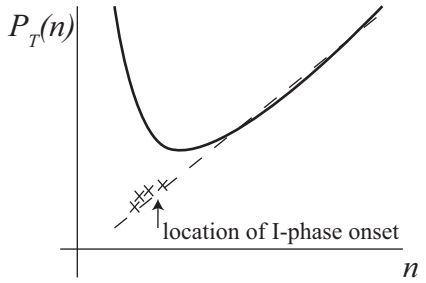

Figure 16. Schematic cartoon of the power threshold dependency on n. I-phase onset is roughly observed on the low n extrapolation of the high n linear proportionality.